Graphene/Pentacene Barristor with Ion-Gel Gate Dielectric: Flexible Ambipolar Transistor with High Mobility and On/Off Ratio

Gwangtaek Oh,[†] Jin-Soo Kim,[†] Ji Hoon Jeon,[†] EunA Won,[†] Jong Wan Son,[†] Duk Hyun Lee,[†] Cheol Kyeom Kim,[†] Jingon Jang,[‡] Takhee Lee,[‡] and Bae Ho Park*,[†]

[†]Division of Quantum Phases & Devices, Department of Physics, Konkuk University, Seoul 143-701, Korea and [‡]Department of Physics and Astronomy, and Institute of Applied Physics, Seoul National University, Seoul 151-747, Korea

ABSTRACT High-quality channel layer is required for next-generation flexible electronic devices. Graphene is a good candidate due to its high carrier mobility and unique ambipolar transport characteristics but typically shows a low on/off ratio caused by gapless band structure. Popularly investigated organic semiconductors, such as pentacene, suffer from poor carrier mobility. Here, we propose a graphene/pentacene channel layer with high-k ion-gel gate dielectric. The graphene/pentacene device shows both high on/off ratio and carrier mobility as well as excellent mechanical flexibility. Most importantly, it reveals ambipolar behaviors and related negative differential resistance, which are controlled by external bias. Therefore, our graphene/pentacene barristor with ion-gel gate dielectric can offer various flexible device applications with high performances.

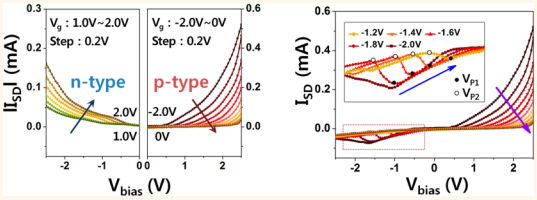

KEYWORDS: graphene/pentacene barristor · ion-gel gate dielectric · flexible and ambipolar transistor · high mobility and on/off ratio · negative differential resistance

Graphene, a two-dimenstional atomic crystal made of carbon, has attracted significant interest for electronics applications due to its high intrinsic carrier mobility, excellent mechanical flexibility, optical transparency, and unique ambipolar transport characteristic.[1,2] Especially, ambipolarity implies that carriers can be tuned continuously between holes and electrons by supplying the requisite gate biases and enables a wide array of applications including frequency multipliers, memory, fast switches, and high-frequency oscillators up to the terahertz (THz) range.[3−6] However, its gapless band structure gives rise to low on/off ratio in a graphene-based transistor[2,7−9] whose implementation in real applications has yet to occur.

High on/off ratio has been achieved by introducing a barristor,[1,2] that is a gated graphene/semiconductor junction, because its high junction resistance can provide sufficiently low off-state current.[10,11] However, such a barristor has usually lost the benefits of graphene, such as mechanical flexibility, optical transparency, and the ambipolar transport properties because rigid and opaque unipolar semiconductor and low-k dielectric have been used.[3−6]

Here, we make a contact of graphene and pentacene,[12−17] which is a flexible and transparent ambipolar semiconductor, and employ a high-k ion-gel dielectric to implement a flexible ambipolar barristor.[7,8,18−23] The graphene/pentacene barristor maintains its resistance value when up to 4.0% bending strain is applied. It exhibits high on/off ratio of 10^4 and mobility 100 times higher than that of pure pentacene device. The modulation of graphene's Fermi level (E_F) by applying gate voltage (V_g) is confirmed by the change in Schottky barrier height (φ_b) at the graphene/pentacene junction. Most strikingly, we can observe ambipolar transfer curves and negative differential resistance (NDR) behaviors in the graphene-based barristor, which are unprecedented. The NDR behaviors are well-fitted using a transport model of a graphene channel with a p−n junction caused by potential gradient.

* Address correspondence to baehpark@konkuk.ac.kr.

Received for review May 1, 2015 and accepted June 17, 2015.

Published online June 17, 2015
10.1021/acsnano.5b02616

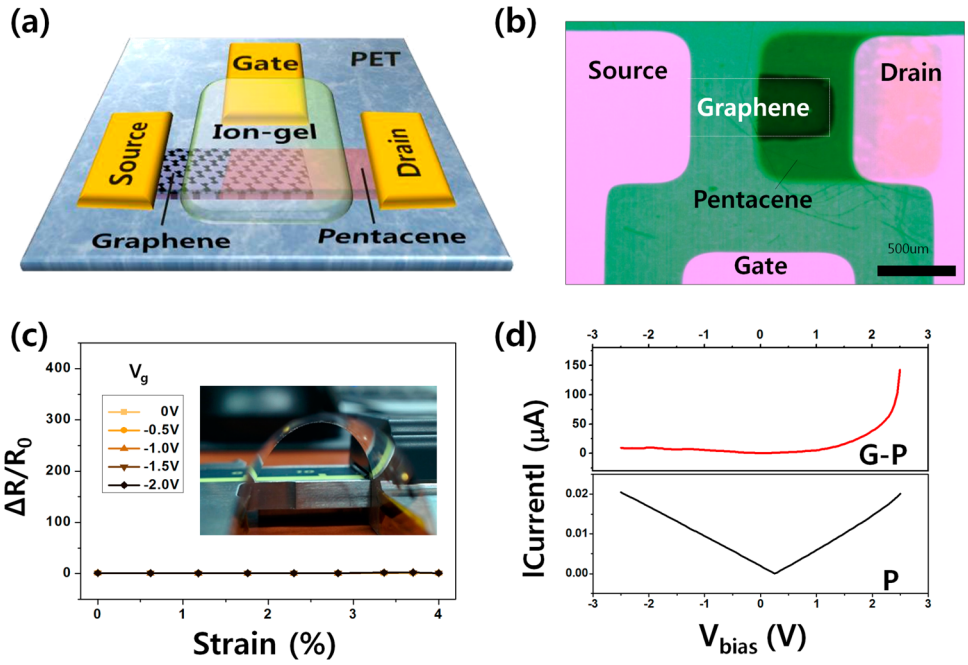

Figure 1. Graphene/pentacene barristor characterization. (a) A schematic diagram and (b) an optical microscope image of a graphene/pentacene barristor. (c) Ratio of resistance change to initial resistance value of a graphene/pentacene barristor under bending strain. The inset shows the photograph of a strained barristor/PET structure. (d) $|I_{SD}|-V_{bias}$ characteristic of a graphene/pentacene barristor (red) and a pure pentacene device (black) at V_g = 0 V.

RESULTS AND DISCUSSION

Figure 1a,b shows a schematic diagram and an optical microscope image, respectively, of the graphene/pentacene barristor structure fabricated on polyethylene terephthalate (PET) substrate. Ion-gel was used as a gate dielectric because ion-gel was known as an ideal dielectric material for field effect devices.[7,8,22,23] As a reference device, we also fabricated a side-gate pure pentacene device with the same dimension. We measured resistance value of graphene/pentacene on PET between source and drain electrodes at a reading voltage of 0.3 V by applying external mechanical stress on it, as shown in the inset of Figure 1c. Figure 1c shows the ratio of resistance change to initial resistance value of a graphene/pentacene barristor under bending strain. Bending strain was applied to graphene/pentacene device on PET (188 μm) and can be calculated from the following equation[24,25]

$$\varepsilon = \left(\frac{\delta_s + \delta_f}{2R_C}\right)\frac{(1 + 2\eta + \chi\eta^2)}{(1 + \eta + \chi\eta + \chi\eta^2)} \qquad (1)$$

where $\eta = \delta_f/\delta_s$, $\chi = Y_f/Y_s$, and R_C is the bending radius. δ is thickness and Y is Young's modulus. The subscripts s and f indicate, respectively, substrate (PET) and film (graphene) which is in direct contact with the substrate. The graphene/pentacene barristor reveals negligible change in resistance value at up to ~4% bending strain (corresponding to a bending radius of 4.0 mm). This result is comparable to those of pure pentacene and graphene devices.[24,26] It seems that the graphene/pentacene barristor exhibits good optical transparency and excellent mechanical flexibility (see Supporting Information).

We measured current−voltage ($I_{SD}-V_{bias}$) characteristics between source and drain to confirm formation of the Schottky barrier at the graphene/pentacene interface. While black line in Figure 1d shows a symmetric $|I_{SD}|-V_{bias}$ curve of a pure pentacene device, red line reveals a rectifying curve of a graphene/pentacene barristor device, which is a typical feature of a graphene/p-type semiconductor barristor.[11] It is noticeable that I_{SD} of a graphene/pentacene barristor device is higher than that of a pure pentacene device by more than 1 order of magnitude even in the reverse bias region of Figure 1d.

If we could electrostatically modulate the graphene's E_F by applying V_g, φ_b would be changed at the graphene/pentacene junction. Because the injection of the majority carriers from graphene to pentacene is affected by φ_b, V_g is expected to directly control the magnitude of I_{SD}. Figure 2a shows $I_{SD}-V_{bias}$ curves of a graphene/pentacene barristor device when V_g, which varies from −2.0 to 0 V with a step size of 0.2 V, is applied from a side gate. The large modulation of I_{SD} is indicative of a large variation in φ_b, caused by the electric field effect derived from V_g. The most significant feature of the Figure 2a is the repression of I_{SD} in the positive V_{bias} region as V_g increases from −2.0 to 0 V, which is usually observed for a graphene/p-type semiconductor barristor.

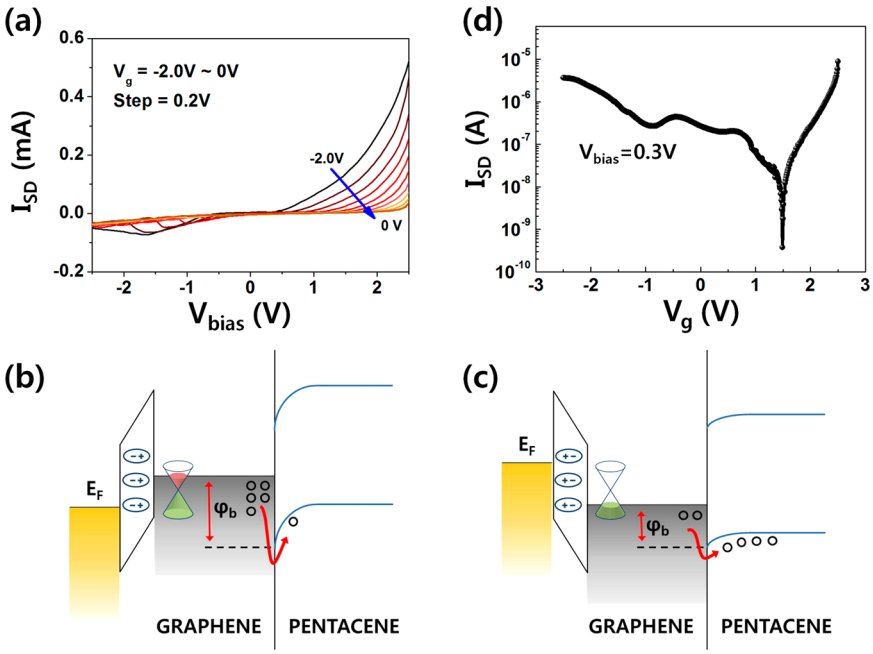

Figure 2. Field effect on a graphene/pentacene barristor. (a) $I_{SD}-V_{bias}$ curves of a graphene/pentacene barristor device when V_g, which varies from −2.0 to 0 V with a step size of 0.2 V, is applied from a side gate. The blue arrow indicates the direction of increasing V_g. Schematic band diagrams of a graphene/pentacene barristor when a (b) positive and (c) negative V_g is applied. (d) Transfer characteristics of a graphene/pentacene barristor, which is measured as a function of V_g at a fixed V_{bias} = 0.3 V.

Figure 2b,c shows schematic band diagrams of a graphene/pentacene barristor where pentacene is assumed to be a p-type semiconductor. This is reasonable because pentacene is typically considered as a p-type semiconductor and our graphene/pentacene barristor device shows p-type characteristics without V_g in Figure 1d. Positive V_g elevates E_F of graphene, leading to increase in φ_b at graphene/pentacene interface and thus decrease in charge carrier transport. In contrast, negative V_g lowers E_F of graphene, leading to decrease in φ_b at graphene/pentacene interface and thus increase in charge carrier transport. As a result, the forward current across the Schottky barrier decreases as V_g increases from −2.0 to 0 V (Figure 2a).

To check transfer characteristics of the graphene/pentacene barristor device, forward diode current was measured as a function of V_g at a fixed V_{bias} = 0.3 V, as shown in Figure 2d. Our graphene/pentacene barristor device shows high on/off ratio of 10^4 which substantially exceeds those in the range of 2−20 reported for pure graphene transistors.[21] In addition, field effect mobility of our graphene/pentacene barristor is much higher than that of our pure pentacene device by 3 orders of magnitude. It is reported that typical pentacene devices have low mobility values ranging from 0.21 to 2.20 $cm^2/(V\ s)$.[14,15] The most striking result is that the $I_{SD}-V_g$ curve of our graphene/pentacene barristor shows an ambipolar behavior involving both positive and negative majority charge carriers. Up to now, it has been reported that barristor consisting of a graphene/semiconductor junction always shows a unipolar behavior concerned with only one kind of majority carrier.[10,11] Although ambipolar electric field effect of graphene underlies a large number of works studying its electronic transport as well as sensing and other device-related applications, unipolar behaviors of graphene/semiconductor barristor devices have limited their versatile applications. Therefore, ambipolar behavior of our graphene/pentacene barristor can contribute to overcoming limitation and extending application of barristor based on graphene.

In a pure organic semiconductor device with ion-gel dielectric,[6,33] typical $I_{SD}-V_g$ curve shows either suppressed current region due to a considerable bandgap of ambipolar organic semiconductor or negative transconductance region by accumulation. Our pure graphene device without pentacene junction showed sublinear $I_{SD}-V_g$ curve whose minimum shifts to positive V_g due to local perturbations from substrate (PET), gate dielectric material (ion-gel), and junction material (pentacene).[6,18,22] Because our barristor device consists of graphene and pentacene in series, nonmonotonic current increase in the left branch (p-branch) of the $I_{SD}-V_g$ curve can be observed in the suppressed current or negative transconductance region of pentacene. In contrast, $I_{SD}-V_g$ curve of our barristor device shows monotonic current increase outside the suppressed current or negative transconductance region of pentacene (in the p-branch under strongly negative V_g or n-branch).

To further investigate ambipolar characteristics of a graphene/pentacene barristor device, we apply V_g with wider range from −2.0 to 2.0 V (0.2 V step) when we measure $|I_{SD}|-V_{bias}$ curves. The right panel of

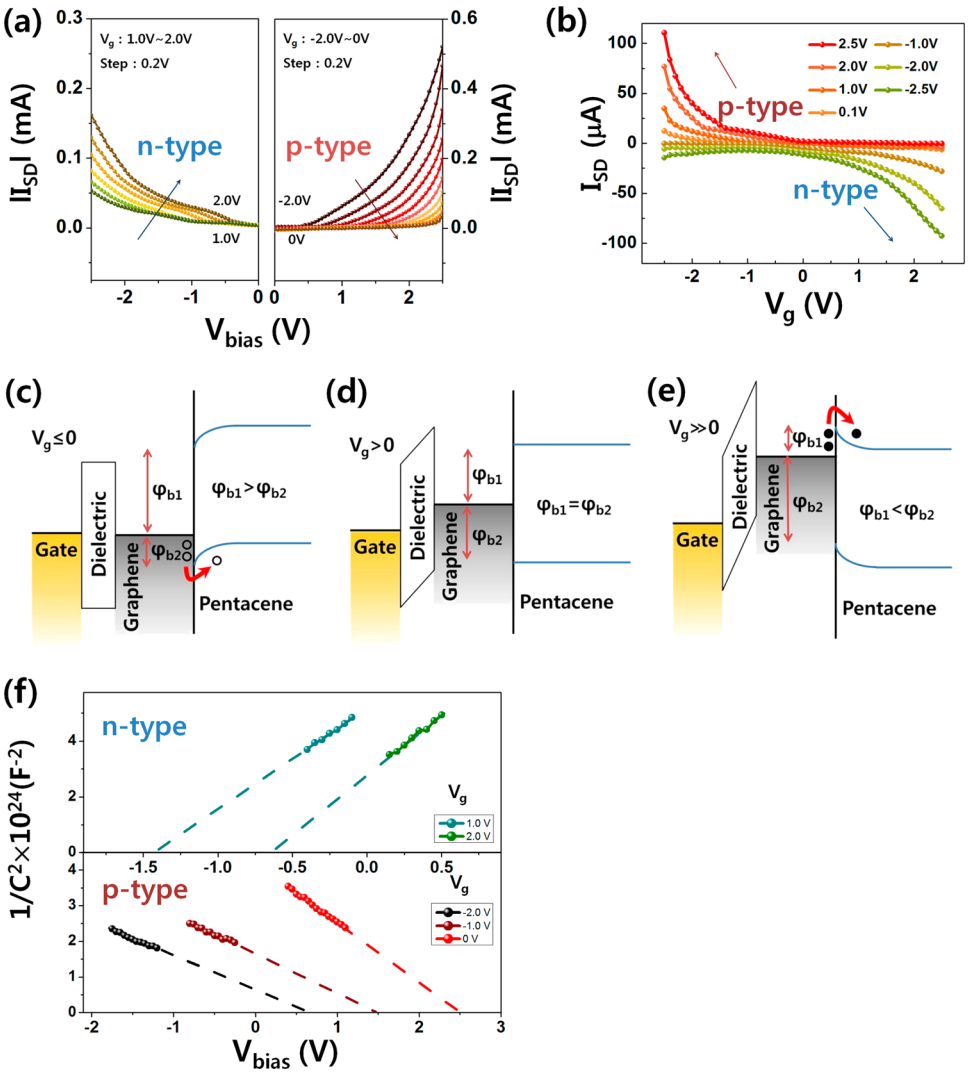

Figure 3. Ambipolarity of a graphene/pentacene barristor. (a) $|I_{SD}|-V_{bias}$ curves measured as V_g increases from −2.0 to 0 V (right panel) and from 1.0 to 2.0 V (left panel), respectively, with 0.2 V step. (b) Transfer characteristics in the V_g sweeping from −2.5 to 2.5 V at a fixed V_{bias} (−2.5 to 2.5 V with 0.5 V step). The red and blue arrows indicate directions of increasing current magnitude in p-type and n-type regions, respectively. Schematic band diagram of a graphene/pentacene barristor at (c) $V_g \leq 0$, (d) $V_g > 0$, and (e) $V_g \gg 0$. (f) C^{-2} *versus* V_{bias} plots of a graphene/pentacene junction in reverse bias region under various V_g values.

Figure 3a shows the repression of $|I_{SD}|$ as V_g increases from −2.0 to 0 V in the positive V_{bias} region, which is typically observed in a p-type barristor. The left panel of Figure 3a reveals the enhancement of $|I_{SD}|$ as V_g increases from 1.0 to 2.0 V in the negative V_{bias} region, which is manifested in an n-type barristor.[10]

The ambipolar behaviors of a graphene/pentacene barristor are confirmed by measuring transfer characteristics in the V_g sweeping from −2.5 to 2.5 V at a fixed V_{bias} (−2.5 to 2.5 V with 0.5 V step), as shown in Figure 3b. At negative V_g region, we can observe p-type barristor features: $|I_{SD}|$ decreases as V_g increases from −2.5 to 0 V, which is more distinct at positive V_{bias} than at negative V_{bias}. At positive $V_g > 1.0$ V, we can observe n-type barristor features: $|I_{SD}|$ increases as V_g increases from 1.0 to 2.5 V, which is more obvious at negative V_{bias} than at positive V_{bias}. It is noteworthy that we can control the type of a graphene/pentacene barristor device by changing applied V_g similarly to an ambipolar graphene channel device.

The observed ambipolar characteristics controlled by V_g can be explained using band diagrams in Figure 3c–e. φ_{b1} and φ_{b2} indicate barrier heights for electrons and holes, respectively, formed at a graphene/pentacene interface. Given that our graphene/pentacene barristor reveals p-type characteristics at $V_g = 0$ V in Figure 3a, we can assume that $\varphi_{b1} > \varphi_{b2}$ at $V_g = 0$ V as shown in Figure 3c. Hole becomes a majority carrier because it can be more easily injected to pentacene than electron. Applied positive V_g can elevate the E_F of graphene compared to that of pentacene due to small area of graphene Fermi surface.[2] Therefore, we can obtain positive V_g values which render $\varphi_{b1} = \varphi_{b2}$ and further $\varphi_{b1} < \varphi_{b2}$ as shown in

Figure 3, panels d and e, respectively. When $\varphi_{b1} < \varphi_{b2}$ at $V_g \gg 0$, electron becomes a majority carrier and the graphene/pentacene barristor exhibits n-type characteristics as shown in Figure 3a.

Such an ambipolar behavior has not been reported in conventional graphene barristors, although it is one of the most interesting features of graphene. Our graphene/pentacene device is the first discovered graphene-based barristor which maintains the promising ambipolar performance of graphene. It seems that the observed ambipolar behavior of our graphene/pentacene device may be caused by high capacitance ($\sim$20 μF/cm^2) of ion-gel gate dielectric, small band gap ($\sim$1.9 eV) of pentacene, and ambipolar characteristics of graphene and pentacene. Because ion-gel gate dielectrics have usually 500 times higher capacitance than those of conventional oxide gate dielectrics (SiO_2: $\sim$0.035 μF/cm^2),[6] graphene's E_F can be modulated to a large extent when ion-gel gate dielectric is introduced. Small values of φ_{b1} and φ_{b2} are caused by small band gap of pentacene leading to facile control of inequality sign between φ_{b1} and φ_{b2} through modulation of graphene's E_F. Theoretical and experimental studies have reported that pentacene is an ambipolar material with similarly high mobility values of holes and electrons, which can become either p-type or n-type channel by accumulating either holes or electrons, respectively, depending on the sign of V_g.[3−6] In practice, two basic requirements must be met to achieve the ambipolar characteristics of pentacene: first, use of appropriate gate dielectrics with minimum density of electron and hole traps; second, use of suitable source and drain electrodes for both electron and hole injections at the interface between pentacene and electrodes. We infer that the two requirements are satisfied in our graphene/pentacene barristor by using both ion-gel as a gate dielectric material and ambipolar graphene as a contact to the source electrode.

We performed capacitance−voltage ($C-V$) measurement for our graphene/pentacene barristor in order to confirm the control of graphene's E_F with applied V_g. If reverse bias (V_R) is applied to a Schottky barrier, the solution to Poisson's equation in the depletion region gives the relation,[27]

$$\frac{1}{C^2} = \frac{2(V_{bi} + V_R)}{(eN_D\epsilon_s)} \quad (2)$$

where e, N_D, and ε_s are the elementary charge, doping concentration of donors (n-type) or acceptors (p-type), and the dielectric constant of semiconductor, respectively. The "built in" potential energy eV_{bi} is a semiconductor band bending at a metal/semiconductor interface compared to the flat band at neutral region in the semiconductor. Figure 3f displays C^{-2} *versus* V_R plots of a graphene/pentacene junction under various V_g values, which are measured at 1 MHz and room temperature. Lower and upper panels reveal typical linear relationships of C^{-2} *versus* V_R for Schottky junctions formed at metal/p-type and metal/n-type semiconductors, respectively. From the x-intercept of each linear fitting line of the corresponding data, we can determine V_{bi} of the graphene/pentacene junction under a specific V_g: 0.64 and 1.46 eV under V_g of −2.0 and −1.0 V, respectively, in p-type region (lower panel); −1.40 and −0.64 eV under V_g of 1.0 and 2.0 V, respectively, in n-type region (upper panel). The positive and negative V_{bi} values, respectively, indicate the downward and upward band bending of pentacene at the graphene/pentacene interface.

Using the following equations, we can estimate φ_b's at metal/n-type and metal/p-type semiconductor junctions.

$$\varphi_b = \frac{eV_{bi}}{n} + (E_C - E_F) \quad (3)$$

$$\varphi_b = \frac{eV_{bi}}{n} + (E_F - E_V) \quad (4)$$

where n is the diode ideality factor. The difference between the conduction band minimum (E_C) and E_F is 1.33 eV and the difference between E_F and the valence band maximum (E_V) is 0.57 eV for a neutral pentacene.[16,17,28,29] Therefore, we can determine φ_b at our graphene/pentacene junction under a specific V_g: 0.74 and 0.97 eV under V_g of −2.0 and −1.0 V, respectively, in p-type region; 1.71 and 1.50 eV under V_g of 1.0 and 2.0 V, respectively, in n-type region. In p-type region, barrier height for holes (φ_{b2}) increases as V_g increases from −2.0 to −1.0 V. In n-type region, barrier height for electrons (φ_{b1}) decreases as V_g increases from 1.0 to 2.0 V. These results demonstrate that E_F of graphene is modulated by applied V_g leading to ambipolar characteristics of a graphene/pentacene barristor with a tunable φ_b.

Figure 4a shows $I_{SD}-V_{bias}$ curves of a graphene/pentacene barristor device when V_g, which varies from −2.5 to 1.0 V with step size of 0.2 V, is applied. Surprisingly, NDR phenomena are observed in negative V_{bias} regions when applied V_g ranges from −2.0 to −1.2 V (inset of Figure 4a). It was reported that NDR effect was achieved in chemically modulated asymmetric graphene diodes[30] and ascribed to both ambipolar transport property of graphene and existence of a minimum sheet carrier density at the second inflection voltage point (V_{P2}) in graphene channel.[31] First inflection voltage point (V_{P1}) is a starting voltage of NDR phenomena. $|V_{P1}|$ and $|V_{P2}|$ of our graphene/pentacene device decrease as V_g is elevated as shown in the inset of Figure 4a.

Graphene transport model is applied to our graphene/pentacene barristor device.[32] We should note that our graphene/pentacene device structure is different from that of a conventional graphene channel device: graphene in contact with source metal;

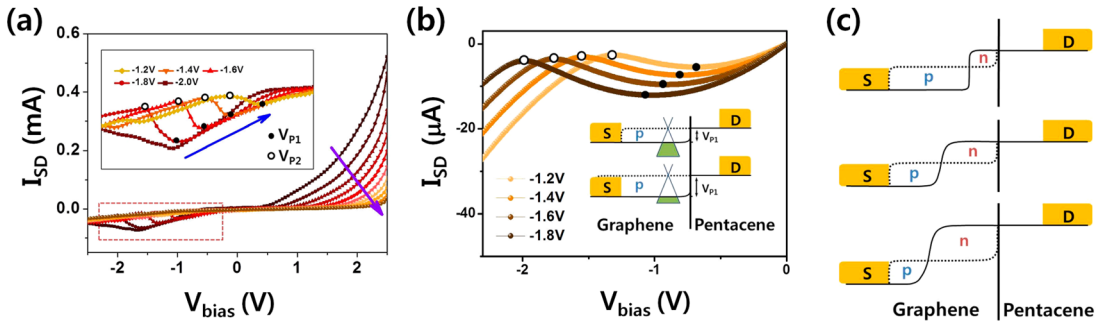

Figure 4. NDR phenomena of a graphene/pentacene barristor. (a) $I_{SD}-V_{bias}$ curves of a graphene/pentacene barristor device when V_g, which varies from −2.5 to 1.0 V with step size of 0.2 V, is applied. The inset shows the magnified curves. V_{P1} and V_{P2} are the first and second inflection voltage, respectively. (b) $I_{SD}-V_{bias}$ simulation results obtained using graphene transport model as a function of V_g ranging from −1.8 to −1.2 V. The inset shows band diagrams at $V_{bias} = V_{P1}$. (c) Band diagrams at $V_{bias} < V_{P1}$ (top), $V_{bias} = V_{P2}$ (middle), and $V_{bias} < V_{P2}$ (bottom), when NDR phenomena come about.

pentacene in contact with drain metal; graphene/pentacene junction inside channel covered by ion-gel gate dielectric. Applied V_g changes carrier density of both graphene and pentacene inevitably in our device. Asymmetric carrier concentration inside the graphene channel is caused by the graphene/pentacene junction. The graphene channel current at a finite V_{bias} is expressed as,

$$I_{SD} = \frac{W}{L} KV_{bias}\sqrt{(V_g - \alpha V_{bias})^2 + \left(\frac{\sigma_{min}}{K}\right)^2} \quad (5)$$

where $K = C\cdot\mu$ is the product of the gate capacitance and carrier mobility, σ_{min} is the conductance minimum, and α ($0 < \alpha < 1$) is the coefficient of transport asymmetry between electrons and holes. In this analytic expression, the NDR effect is prominent when σ_{min}/K value is below 1.[32] In our devices, K value is obtained by calculating the field effect mobility using following relation.

$$\mu = \frac{L}{W} m_{lin}\frac{1}{C}\frac{1}{V_{bias}} \quad (6)$$

where W/L ratio is 1 and m_{lin} is the slope of the linear fit in $I_{SD}-V_g$ curve (see Supporting Information). Using the measured value of $\sigma_{min}/K = 0.153$ in conjunction with $\alpha = 0.9$, simulation results (Figure 4b) as a function of V_g ranging from −1.8 to −1.2 V exhibit good agreement with the experimental data.

At negative V_{bias} close to 0, the dominant carriers in the channel are holes injected from the source with a carrier density controlled by V_g. Therefore, the resistance in graphene channel is nearly constant in position and the graphene/pentacene device exhibits Ohmic-like $I_{SD}-V_{bias}$ behavior. As V_{bias} decreases and becomes equal to V_{P1} (inset of Figure 4b), the local Fermi energy at the graphene/pentacene junction coincides with the Dirac point of graphene. Since the local channel resistivity is inversely proportional to the local carrier density, it is highest at the junction where most of the voltage drop occurs. If more negative V_g is applied, larger $|V_{P1}|$ is required for elevating lower E_F to Dirac point at the junction as shown in the inset of Figure 4b.

NDR behavior can be qualitatively understood from the evolution of the carrier distribution in the graphene channel as V_{bias} varies, as depicted in Figure 4c. The top of Figure 4c illustrates the band diagram of the graphene channel when negative V_{bias} lower than V_{P1} is applied. It is noted that the majority carrier close to the junction is changed to electrons injected from the drain while that close to the source is still holes. As shown in the middle of Figure 4c, n-type region in graphene expands as V_{bias} decreases. Thus, the total channel resistance increases until the distribution of electron and hole carriers becomes symmetric along the graphene when $V_{bias} = V_{P2}$ because part of the hole-dominated channel is replaced by an electron-dominated region with a lower carrier density and higher resistance. We can easily expect that $|V_{P2}|$ increases as applied V_g decreases and E_F of graphene is lowered. The bottom of Figure 4c depicts the band diagram when V_{bias} is less than V_{P2}. In this case, the total channel resistance is lower than that of the middle of Figure 4c due to two factors: (1) the decrease of electron-dominated channel resistance due to increasing electron carrier density and (2) replacement of part of the hole-dominated channel by the electron-dominated region with lower resistance.[32] We should note that NDR phenomena are induced by extending n-type region in an initially p-type doped graphene with the aid of applied negative V_{bias}. However, NDR phenomena are not observed at positive V_{bias} which cannot generate n-type region in the p-type graphene.

CONCLUSIONS

In conclusion, we fabricate a graphene/pentacene barristor with a high-k ion-gel gate dielectric on a PET substrate. It overcomes disadvantages of both graphene and pentacene, which are low on/off ratio and mobility, respectively. In contrast to a conventional

graphene/semiconductor barristor, the graphene/pentacene barristor clearly shows ambipolar behaviors and NDR controlled by external bias as well as excellent mechanical flexibility. Therefore, it can be a good candidate for a flexible ambipolar transistor with high mobility and on/off ratio.

METHODS

Single-layer graphene fabricated by chemical vapor deposition was transferred on PET and etched to a rectangular shape by oxygen plasma using a metal shadow mask. To make a graphene/pentacene junction, pentacene film (300 nm thickness) with a rectangular shape was deposited through a metal shadow mask by a thermal evaporator with a deposition rate of 0.5 Å/s at a pressure of 10^{-6} Torr. Au(50 nm)/Cr(5 nm) source, drain, and gate electrodes were, respectively, deposited on graphene, pentacene, and PET through a metal shadow mask by an e-beam evaporator.

The ion-gel was fabricated by the gelation of a triblock copolymer in an ionic liquid. A UV cross-linkable polyelectrolyte ion-gel dielectric layer was deposited on the graphene/pentacene structure as a gate dielectric. 1-Ethyl-3-methylimidazolium bis(trifluoromethylsulfonyl)imide [EMIM][TFSI] ionic liquid, poly(ethylene glycol) diacrylate (PEG-DA, Mw = 575) monomer, and 2-hydroxy-2-methylpropiophenone (HOMPP, UV cross-linking initiator) were mixed at a weight-ratio of 88:8:4, and the mixed solution was dropped and spread on the graphene/pentacene structure. The dropped solution was solidified by UV exposure (365 nm, 100 mW/cm^2) for 10 s, and a side-gate graphene/pentacene device with channel dimension of 500 μm $\times$ 1000 μm was obtained.

Conflict of Interest: The authors declare no competing financial interest.

Supporting Information Available: Absorption spectra of a graphene/pentacene structure grown on a PET substrate; device characteristics of a graphene/pentacene barristor on SiO_2/Si; methods to calculate parameters of a graphene/pentacene barristor with ion-gel dielectric on a PET substrate; supporting methods and discussion. The Supporting Information is available free of charge on the ACS Publications website at DOI: 10.1021/acsnano.5b02616.

Acknowledgment. This work was supported by the National Research Foundation of Korea (NRF) grants funded by the Korea government (MSIP) (No. 2013R1A3A2042120, 2015001948, and 2011-0030229). T.L. and J.J. thank the financial support from the National Creative Research Laboratory program (Grant No. 2012026372) of Korea. Gwangtaek Oh and Bae Ho Park planned the projects and designed the experiments; Gwangtaek Oh, Ji Hoon Jeon, Jong Wan Son, Duk Hyun Lee, Cheol Kyeom Kim, and EunA Won fabricated and characterized graphene/pentacene barristors; Takhee Lee and Jingon Jang provided pentacene films; Jin-Soo Kim performed and analyzed the calculations; Gwangtaek Oh, Jin-Soo Kim and Bae Ho Park interpreted the results.

REFERENCES AND NOTES

1. Novoselov, K. S.; Fal'ko, V.; Colombo, L.; Gellert, P. R.; Schwab, M. G.; Kim, K. A Roadmap for Graphene. *Nature* **2012**, *490*, 192–200.
2. Han, M. Y.; Kim, P. Graphene Nanoribbon Devices at High Bias. *Nano Convergence* **2014**, *1*, 1.
3. Cornil, J.; Brédas, J.-L.; Zaumseil, J.; Sirringhaus, H. Ambipolar Transport in Organic Conjugated Materials. *Adv. Mater.* **2007**, *19*, 1791–1799.
4. Saudari, S. R.; Lin, Y. J.; Lai, Y.; Kagan, C. R. Device Configurations for Ambipolar Transport in Flexible, Pentacene Transistors. *Adv. Mater.* **2010**, *22*, 5063–5068.
5. Chua, L.-L.; Zaumseil, J.; Chang, J.-F.; Ou, E. C.-W.; P. Ho, K.-H.; Sirringhaus, H.; Friend, R. H. General Observation of N-type Field-Effect Behaviour in Organic Semiconductors. *Nature* **2005**, *434*, 194–199.
6. Yomogida, Y.; Pu, J.; Shimotani, H.; On, S.; Hotta, S.; Iwasa, Y.; Takenobu, T. Ambipolar Organic Single-Crystal Transistors Based on Ion Gels. *Adv. Mater.* **2012**, *24*, 4392–4397.
7. Kim, B. J.; Jang, H.; Lee, S.-K.; Hong, B. H.; Ahn, J.-H.; Cho, J. H. High-Performance Flexible Graphene Field Effect Transistors with Ion Gel Gate Dielectrics. *Nano Lett.* **2010**, *10*, 3464–3466.
8. Chen, C.-F.; Park, C.-H.; Boudouris, B. W.; Horng, J.; Geng, B.; Girit, C.; Zettl, A.; Crommie, M. F.; Segalman, R. A.; Louie, S. G.; Wang, F. Controlling Inelastic Light Scattering Quantum Pathways in Graphene. *Nature* **2011**, *471*, 617–620.
9. Schwierz, F. Graphene Transistors. *Nat. Nanotechnol.* **2010**, *5*, 487–496.
10. Yang, H.; Heo, J.; Park, S.; Song, H. J.; Seo, D. H.; Byun, K.-E.; Kim, P.; Yoo, I.; Chung, H.-J.; Kim, K. Graphene Barristor, a Triode Device with a Gate-Controlled Schottky Barrier. *Science* **2012**, *336*, 1140–1143.
11. Ojeda-Aristizabal, C.; Bao, W.; Fuhrer, M. S. Thin-Film Barristor: A Gate-Tunable Vertical Graphene-Pentacene Device. *Phys. Rev. B* **2013**, *88*, 035435.
12. Jang, J.; Song, Y.; Oh, H.; Yoo, D.; Kim, D.; Lee, H.; Hong, S.; Lee, J.-K.; Lee, T. The Application of Orthogonal Photolithography to Micro-Scale Organic Field Effect Transistors and Complementary Inverters on Flexible Substrate. *Appl. Phys. Lett.* **2014**, *104*, 053301.
13. Tiago, M. L.; Northrup, J. E.; Louie, S. G. Ab Initio Calculation of the Electronic and Optical Properties of Solid Pentacene. *Phys. Rev. B* **2003**, *67*, 115212.
14. Sokolov, A. N.; Atahan-Evrenk, S.; Mondal, R.; Akkerman, H. B.; Sánchez-Carrera, R. S.; Granados-Focil, S.; Schrier, J.; Mannsfeld, S. C. B.; Zoombelt, A. P.; Bao, Z.; et al. From Computational Discovery to Experimental Characterization of a High Hole Mobility Organic Crystal. *Nat. Commun.* **2011**, *2*, 437.
15. Naab, B. D.; Himmelberger, S.; Diao, Y.; Vandewal, K.; Wei, P.; Lussem, B.; Salleo, A.; Bao, Z. High Mobility N-type Transistors Based on Solution-Sheared Doped 6,13-Bis-(triisopropylsilylethynyl)pentacene Thin Films. *Adv. Mater.* **2013**, *25*, 4663–4667.
16. Feng, C.; Mei, T.; Huc, X.; Pavel, N. A Pentacene Field-Effect Transistor with Light-Programmable Threshold Voltage. *Org. Electron.* **2010**, *11*, 1713–1718.
17. Saranyaa, G.; Nairb, S.; Natarajanb, V.; Kolandaivela, P.; Senthilkumar, K. A Theoretical Study of Structural and Electronic Properties of Pentacene/Al(100) Interface. *J. Mol. Graphics* **2012**, *38*, 334–341.
18. Kim, B. J.; Lee, S.-K.; Kang, M. S.; Ahn, J.-H.; Cho, J. H. Coplanar-Gate Transparent Graphene Transistors and Inverters on Plastic. *ACS Nano* **2012**, *6*, 8646–8651.
19. Lee, S. W.; Lee, H. J.; Choi, J. H.; Koh, W. G.; Myoung, J. M.; Hur, J. H.; Park, J. J.; Cho, J. H.; Jeong, U. Periodic Array of Polyelectrolyte-Gated Organic Transistors From Electrospun Poly(3-hexylthiophene) Nanofibers. *Nano Lett.* **2010**, *10*, 347–351.
20. Choi, J.-H.; Lee, S. W.; Kar, J. P.; Das, S. N.; Jeon, J.; Moon, K.-J.; Lee, T. I.; Jeong, U.; Myoung, J.-M. Random Network Transistor Arrays of Embedded ZnO Nanorods in Ion-Gel Gate Dielectric. *J. Mater. Chem.* **2010**, *20*, 7393–7397.
21. Kim, S. H.; Hong, K.; Xie, W.; Lee, K. H.; Zhang, S.; Lodge, T. P.; Frisbie, C. D. Electrolyte-Gated Transistors for Organic and Printed Electronics. *Adv. Mater.* **2013**, *25*, 1822–1846.
22. Ju, L.; Geng, B.; Horng, J.; Girit, C.; Martin, M.; Hao, Z.; Bechtel, H. A.; Liang, X.; Zettl, A.; Shen, Y. R.; et al. Graphene Plasmonics for Tunable Terahertz Metamaterials. *Nat. Nanotechnol.* **2011**, *6*, 630–634.

23. Pu, J.; Yomogida, Y.; Liu, K.-K.; Li, L.-J.; Iwasa, Y.; Takenobu, T. Highly Flexible MoS_2 Thin-Film Transistors with Ion Gel Dielectrics. *Nano Lett.* **2012**, *12*, 4013–4017.
24. Kang, J.; Kim, H.; Kim, K. S.; Lee, S.-K.; Bae, S.; Ahn, J.-H.; Kim, Y.-J.; Choi, J.-B.; Hong, B. H. High-Performance Graphene-Based Transparent Flexible Heaters. *Nano Lett.* **2011**, *11*, 5154–5158.
25. Chen, Z.; Cotterell, B.; Wang, W. The Fracture of Brittle Thin Films on Compliant Substrates in Flexible Displays. *Eng. Fract. Mech.* **2002**, *69*, 597–603.
26. Fukuda, K.; Hikichi, K.; Sekine, T.; Takeda, Y.; Minamiki, T.; Kumaki, D.; Tokito, S. Strain Sensitivity and Durability in P-type and N-type Organic Thin-Film Transistors with Printed Silver Electrodes. *Sci. Rep.* **2013**, *3*, 2048.
27. Tongay, S.; Schumann, T.; Miao, X.; Appleton, B. R.; Hebard, A. F. Tuning Schottky Diodes at the Many-Layer-Graphene/Semiconductor Interface by Doping. *Carbon* **2011**, *49*, 2033–2038.
28. Alahmed, Z. A.; Mansour, S. A.; EnverAydn, M.; Yakuphanoglu, F. Hybrid Photodiodesbasedon 6,13 -Bis(triisopropyl-silylethynyl)pentacene:Poly[2-methoxy-5-(2-ethyl)hexoxy-Phenylenevinylene]/P-Silicon. *Solid State Commun.* **2013**, *163*, 23–27.
29. Hiramoto, M.; Kubo, M.; Shinmura, Y.; Ishiyama, N.; Kaji, T.; Sakai, K.; Ohno, T.; Izaki, M. Bandgap Science for Organic Solar Cells. *Electronics* **2013**, *538*, 2811–2817.
30. Fiori, G. Negative Differential Resistance in Mono and Bilayer Graphene P-N Junctions. *IEEE Electron Device Lett.* **2011**, *32*, 1334–1336.
31. Wang, X.; Xu, H.; Min, J.; Peng, L.-M.; Xu, J.-B. Carrier Sheet Density Constrained Anomalous Current Saturation of Graphene Field Effect Transistors: Kinks and Negative Differential Resistances. *Nanoscale* **2013**, *5*, 2811–2817.
32. Wu, Y.; Farmer, D. B.; Zhu, W.; Han, S.-J.; Dimitrakopoulos, C. D.; Bol, A. A.; Avouris, P.; Lin, Y.-M. Three-Terminal Graphene Negative Differential Resistance Devices. *ACS Nano* **2012**, *6*, 2610–2616.
33. Xia, Y.; Xie, W.; Ruden, P. P.; Frisbie, C. D. Carrier Localization on Surfaces of Organic Semiconductors Gated with Electrolytes. *Phys. Rev. Lett.* **2010**, *105*, 036802.